Polymer 304 (2024) 127095

Contents lists available at ScienceDirect

Polymer

journal homepage: www.elsevier.com/locate/polymer

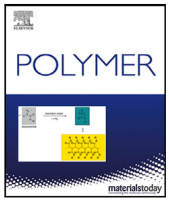

The impact of plasticisers on crystal nucleation, growth and melting in linear polymers

Dominic Wadkin-Snaith, Paul A. Mulheran, Karen Johnston *

Department of Chemical and Process Engineering, University of Strathclyde, Glasgow G1 1XJ, United Kingdom

ARTICLE INFO

Dataset link: https://doi.org/10.15129/3d50ebe5-fc32-4c6a-ade0-b2fbbe054b51

Keywords:
Plasticisers
Fillers
Crystallisation

ABSTRACT

Plasticisers are often added to crystallising polymers to improve their processability. Despite many experimental studies, very few modelling studies have been performed to provide fundamental understanding of the impact of plasticisers on polymer cyrstallisation kinetics and thermodynamics. In this work, molecular dynamics simulations are used to study crystallisation in a model linear polymer with plasticiser. We first demonstrate that the plasticiser lowers the amorphous phase glass transition, with the extent of the effect increasing with plasticiser concentration, due to increased polymer mobility. Using a model filler surface to induce crystallisation, we find that the plasticiser also reduces crystallisation and melting temperatures. Furthermore, we find that the plasticiser is expelled from the crystals during growth so that its concentration in the amorphous matrix increases with degree of crystallisation. This has a pronounced consequence for crystal melting, and we find a broad temperature range where the crystal is in equilibrium with the amorphous phase, which we rationalise in terms of free energy changes. This has potentially important consequences for the processing of linear polymers such as polyhydroxybutyrate (PHB), poly(l-lactic acid) (PLLA) and polyvinyl alcohol (PVA), by providing the opportunity for processing the polymer in a semicrystalline rather than fully amorphous state.

1. Introduction

Plastic pollution and a need to move away from non-renewable oil-derived polymers is driving a transition towards plastics made from sustainable polymers, such as cellulose, poly(l-lactic acid) (PLLA), and polyhydroxyalkanoates (PHAs) [1–3]. However, sustainable polymers often possess poorer barrier, mechanical and processing properties in comparison to their oil-derived counterparts [4,5]. Consequently, fillers are added to improve barrier and mechanical properties by inducing crystal nucleation, and plasticisers are added to improve the processing properties [6–8]. However, plasticisers also affect the polymer crystallisation properties and thus also play a crucial role in influencing the resultant barrier and mechanical properties [9]. Therefore, we need to understand how the plasticisers impact the polymer crystallisation, so that control of the plastic properties can be exerted and optimised for applications.

The effect of plasticiser concentration on the glass transition temperature (T_g), crystallisation temperature (T_c, where crystallisation proceeds at a high rate on cooling) and crystal melting temperature (T_m) have been studied experimentally for a variety of polymers. Generally, T_g, T_c and T_m all decrease when plasticisers are added to the polymer, as observed for a variety of polymers including the sustainable polymers polyhydroxybutyrate (PHB) [10], PLLA [11], and polyvinyl alcohol [12]. As well as an observed depression in T_m in PLLA, the melting peak as measured in differential scanning calorimetry appears to broaden with increased concentration of plasticiser [13], which is a phenomenon of particular interest to work presented here.

A combination of plasticiser and nucleating agent was found to enhance crystallinity on cooling for poly(lactic acid) (PLA) as well as a reduction in T_m [14]. Another study of PLA [15] demonstrated that while the addition of nucleating agent can slightly increase T_m, the combination of plasticiser and nucleating agent leads to lower T_m as compared to neat PLA.

Computational approaches such as molecular dynamics (MD) simulations can be used to gain insight into these effects at a molecular (coarse-grained) or atomistic level. MD simulations have been used to study filler surface-induced crystal nucleation and growth in pure polymer systems [16–23], finding that the surfaces induce nucleation in polymer melts and that the crystallisation temperature is higher than that of homogeneous nucleation. Other studies have investigated clustering and dispersion of plasticisers in filled polymer systems [24], and the effect of plasticisers on glass forming amorphous polymer melts that do not display crystallinity, showing that both plasticiser

* Corresponding author.
E-mail address: karen.johnston@strath.ac.uk (K. Johnston).

https://doi.org/10.1016/j.polymer.2024.127095
Received 22 February 2024; Received in revised form 22 April 2024; Accepted 22 April 2024
Available online 25 April 2024
0032-3861/© 2024 The Author(s). Published by Elsevier Ltd. This is an open access article under the CC BY license (http://creativecommons.org/licenses/by/4.0/).

and anti-plasticiser depress the glass transition temperature T_g [25–27]. However, to the best of our knowledge, there are no simulation studies to date that look at the effect of a plasticiser on crystallising polymer systems.

In this work we build on our previous study of nucleation induced by smooth surfaces [23], and investigate how the addition of plasticiser molecules to filled polymer systems affects crystal nucleation and growth. Using a coarse grained model for polymer chains and plasticisers, where the polymeric monomers and plasticisers are modelled as beads, we reproduce the experimentally observed depression in T_g, T_m and T_c with the addition of plasticiser. We also show that the addition of plasticiser leads to a broadening in temperature of crystal melting, which we rationalise through a free energy argument.

2. Methodology

2.1. Polymer and surface models

Molecular dynamics simulations are used to study the effect of plasticisers on crystal nucleation and growth in polymer melts with filler particles that act as nucleants. The polymer interactions are modelled using a modified Kremer–Grest (KG) model [23] for which all parameters and degrees of freedom are in Lennard-Jones reduced units. Bond stretching potentials are represented by the finite extensible nonlinear elastic (FENE) potential

$$U_{\text{bond}}(r) = -\frac{1}{2}\kappa_r r_0^2 \ln\left[1-\left(\frac{r}{r_0}\right)^2\right] \tag{1}$$

where r is the distance between bonded beads, and $\kappa_r = 30$ and $r_0 = 1.5$ are the FENE parameters. The model also includes the bond angle bending potential

$$U_{\text{angle}}(\theta) = \kappa_\theta\left(1-\cos\left(\theta-\theta_0\right)\right) \tag{2}$$

where θ is the bond angle and κ_θ is the angle potential strength, corresponding to chain stiffness. The constant κ_θ contains the usual factor of $\frac{1}{2}$ as implemented in LAMMPS. Here $\theta_0 = 180^o$ is the equilibrium angle, chosen to favour straight chain segments required for crystal nucleation.

Non-bonded interactions between beads are represented by a shifted Lennard-Jones (LJ) potential which is zero at the cutoff distance of $r_c = 2.5$

$$\begin{aligned} U_{\text{non-bond}}(r) &= 4\epsilon\left[\left(\frac{\sigma}{r}\right)^{12}-\left(\frac{\sigma}{r}\right)^{6}\right]+C \quad r \le r_c \\ &= 0 \quad r > r_c \end{aligned} \tag{3}$$

Here r is the separation between beads and C is chosen such that the potential is zero at r_c. The LJ potential parameters are $\epsilon = 1$ and $\sigma = 1$.

The filler surface is represented by a LJ 9–3 smooth wall potential of the form

$$U_{\text{wall}}(z) = \epsilon_w\left[\frac{2}{15}\left(\frac{\sigma_w}{z}\right)^9-\left(\frac{\sigma_w}{z}\right)^3\right] \tag{4}$$

where z is the perpendicular distance of the bead from the wall, and the wall potential is cutoff and shifted to zero at $r_c = 2.5$. We set $\sigma_w = 1$, and varied ϵ_w to control the strength of the wall-bead interaction. In this work we will use $\epsilon_w = 1.8$ following our previous work [23]. The walls are placed at the top and bottom of the simulation cell.

Plasticisers are included in our model as single beads. They interact with polymer beads via the shifted LJ interaction Eq. (3). For the plasticiser–plasticiser interaction, the LJ potential is cut off at its minimum and shifted to zero, resulting in a purely repulsive interaction between plasticiser beads to prevent their aggregation. The effect of plasticisers on the glass transition and glassy dynamics have been studied using a coarse grained KG model before, and it has been shown previously that beads with diameter smaller than that of the polymer bead have a plasticising effect [25]. For this study we use a plasticiser bead diameter of $\sigma_{\text{plast}} = 0.85$ with a corresponding plasticiser mass of 0.614, smaller than the polymer bead mass of 1. The LJ interactions between polymer and plasticiser beads are calculated using the Lorentz–Berthelot mixing rules, thus $\epsilon_{\text{poly-plast}} = 1$ and $\sigma_{\text{poly-plast}} = 0.925$.

2.2. System setup and simulation details

All simulations were performed with the LAMMPS package [28] and the equations of motion were integrated using the rRESPA (reversible reference system propagator algorithm) multi-timescale integrator. We use a different timestep for bonded and non-bonded interactions; non-bonded interactions are integrated with a timestep of $d\tau* = 0.004$ while bonded interactions are integrated with a timestep of $d\tau* = 0.001\tau*$ where

$$\tau* = \sqrt{\frac{m\sigma^2}{\epsilon}}\tau. \tag{5}$$

is the LJ unit of time, with $m = 1$ being the mass of a bead, $\epsilon = 1$ and $\sigma = 1$ as defined above, and τ is the simulated time. We use a reduced dimensionless temperature T^*, which is defined as $k_B T/\epsilon$. From here onwards we simply refer to the dimensionless time and temperature as τ and T. For both the NVT and NPT simulations the temperature is controlled by the Nose–Hoover thermostat with a damping time set to 2 τ. For the NPT simulations the pressure is controlled by the Nose–Hoover barostat at $P = 0$ with a damping time of 2 τ. We note that the equilibration protocol used in this work is different to the protocol used in our previous work [23], due to the inclusion of the small plasticiser beads which require a $P = 1$ NPT simulation to encourage mixing. For the NPT simulations, the simulation box is fixed in the y and z dimensions and allowed to vary in the x dimension.

To set up the simulations a 20-bead chain is first relaxed in a vacuum. The coiled chain is then inserted into a simulation box with a random position and orientation. This process is repeated until the simulation box contains 800 chains. Plasticiser beads are inserted into the simulation box at random positions as required. 1303 beads are inserted for 5%, 2606 beads for 10% system and 3909 beads for 15% system, where the percentage is to be understood as mass fraction, although the mass is directly proportional to bead volume. For the bulk simulations of pure polymer and polymer–plasticiser mixtures, the simulation box size is $30.817\times30.817\times30.817\ \sigma^3$, and periodic boundary conditions are applied in the x, y and z directions. To equilibrate the bulk systems we performed a series of simulations at $T = 1.0$. First, a Langevin dynamics simulation was run for 1×10^6 steps with a damping parameter of 100τ, followed by a short NVT run of 1×10^4 steps and then a NPT run with $P = 1$ for 3×10^5 steps. Finally, the density was equilibrated with an NPT run at $P = 0$ for 1×10^7 steps.

To set up simulations with filler surfaces, 800 coiled chains were randomly inserted into a simulation box with dimensions $26.817\times26.817\times30.817\ \sigma^3$. For polymer–plasticiser systems, the plasticiser beads were then randomly inserted into the simulation. LJ 9–3 smooth wall potentials, as described in Eq. (4), were placed at the top and bottom of the simulation box (in the x–y plane). The interaction strength of the bottom wall at $z = 0$ was set to $\epsilon_w = 1.80$, which was previously shown to induce nucleation in the pure polymer system [23], and the interaction strength at the top wall at $z = 30.817$ was set to $\epsilon_w = 0.1$, which was chosen to be a weak interaction so that the top wall was unlikely to induce nucleation while still confining the polymer chains and plasticiser beads. Periodic boundary conditions were applied in the x and y directions. The systems were equilibrated at $T = 1.0$ by first performing an NVT simulation for 1×10^4 steps, followed by an NPT run with $P = 1$ for 3×10^4 steps. Finally, the density was equilibrated with an NPT run at $P = 0$ for 1×10^7 steps.

Cooling simulations were performed for the bulk polymer–plasticiser systems. After equilibration at T = 1.0, the bulk systems were cooled at $P = 0$ from $T = 1.0$ to $T = 0.25$ for 1.875×10^8 steps, corresponding to a cooling rate of $\Gamma_0 = 10^{-6}\ T\ \tau^{-1}$.

Isothermal simulations of polymer and polymer–plasticiser mixtures in bulk and with the walls were also performed at $T = 0.61$ and $T = 0.97$.

For the bulk isothermal simulations at $T = 0.61$, the equilibrated systems at $T = 1.0$ were quenched to $T = 0.61$ where the temperature ramp was performed over 5×10^4 steps. Isothermal NVT simulations were then performed at $T = 0.61$ for 2.5×10^5 steps. A similar procedure was used for the isothermal simulations at maximum growth rate temperatures.

For the isothermal simulations with walls, the equilibrated systems at $T = 1.0$ were quenched to $T = 0.61$ using an NPT run, where the temperature ramp was performed over 5×10^4 steps. Isothermal NPT simulations, which allowed the density to change upon crystallisation, were then performed at $T = 0.61$ for 2.125×10^8 steps. For the isothermal simulations of bulk and wall systems at $T = 0.97$, a LAMMPS restart file was taken from the bulk cooling simulation at $T = 0.97$, and then equilibrated by running an NPT simulation for 2.5×10^5 steps. The isothermal NVT simulation was run for 2.5×10^5 steps.

To simulate melting, we took the end of the isothermal simulations at $T = 0.61$ as a starting point, and then heated the systems at a rate of Γ_0. Each system was heated until all crystal structures were melted and the system was in the melt phase.

2.3. Analysis

Simulations were visualised using VMD [29]. For a quantitative analysis of crystal fraction, the number of beads belonging to straight segments of chains were counted. This approach measures every bond angle, θ, for every polymer in the simulation and labels the central bead defining a given bond angle as "straight" if the angle is greater than $\theta_{\text{cut}} = 162°$ as described in our previous work [23]. In this work a stem is defined as four or more beads that labelled as "straight". The fraction of beads belonging to stems is then used to calculate the stem mass fraction, which is an indication of the degree of crystallinity of the system.

To analyse how polymer chain dynamics are affected by the addition of plasticiser we calculate the dynamical auto-correlation of a bond vector using

$$B_n(t) = \left\langle L_n\left(\frac{\vec{b}(t)\cdot\vec{b}(0)}{|\vec{b}(t)|\,|\vec{b}(0)|}\right)\right\rangle \tag{6}$$

Here $\vec{b}(t)$ is the bond vector at time t, L_n is the nth Legendre polynomial; see Supplementary Information (SI) for more details. We measure $B_n(t)$ for $n = 1$ as this can be related to experiment through the measurement of dielectric relaxation [30] while quantifying orientation decorrelation. To aid comparison, correlation functions were fitted to a Kohlrausch–Williams–Watts (KWW) function of the form

$$\phi(t) = \exp\left[-\left(\frac{t}{\tau_1}\right)^{\beta}\right] \tag{7}$$

where the characteristic decay time, τ_1, and the stretching exponent, β, are used as fitting parameters. The KWW stretched exponential relaxation is well known to describe the decay of correlation functions for heterogeneous systems and is often applied to polymer melts and their associated relaxation processes.

3. Results

In this section we first explore the effect of varying plasticiser concentration on bulk properties such as density and T_g as well as chain mobility before investigating the effect of plasticiser concentration on isothermal lamella growth.

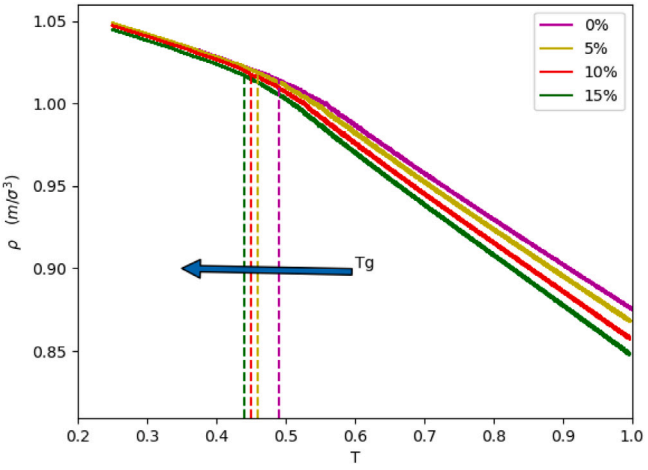

Fig. 1. Density during cooling as a function of plasticiser concentration.

3.1. Effect of plasticiser concentration on bulk polymer properties

Bulk melt simulations with varying concentrations of plasticiser are cooled from $T = 1.0$ to $T = 0.25$ at a rate of Γ_0 in the NPT ensemble. The variation of density with temperature is shown in Fig. 1 for different plasticiser concentrations. Here the plasticiser concentration, c_0, refers to its value in the melt state; as we will see later, the concentration in the amorphous phase of a semicrystalline system will be higher than this.

Firstly, we note that for temperatures above T_g the density decreases as the plasticiser concentration increases. For the highest mass concentration of plasticiser (15 %) the density remains lower than the pure system for temperatures below T_g. The lower density for the plasticised systems indicates an increase in system free volume.

We also observe that as plasticiser mass concentration increases, T_g decreases to lower temperatures, which is consistent with experimentally observed plasticiser behaviour [31–35]. We estimate T_g for the systems with 0%, 5%, 10% and 15% plasticiser to be 0.49, 0.46, 0.45 and 0.44, respectively, although we note that a more accurate estimate of T_g would require a thorough statistical analysis [36].

To analyse the properties of these systems further, we performed isothermal simulations at temperatures of $T = 0.97$, which is well above T_g, and $T = 0.61$, which is still above but closer to T_g. The effect of plasticiser concentration on local chain mobility and bond reorientation relaxation was evaluated using the dynamic bond autocorrelation $B_1(\tau)$, as shown in Fig. 2. It is clear that the decorrelation is much slower at lower temperatures, and a clear dependence on plasticiser concentration can be seen, particularly at $T = 0.61$.

To compare the rate at which local bonds reorientate, as measured by $B_1(\tau)$, we performed a fit of the isothermal relaxation data to a KWW function defined in Eq. (7). The fitting parameters, τ_1 and β, are displayed in Tables 1 and 2 for $T = 0.97$ and $T = 0.61$ respectively, at the various plasticiser concentrations. At both temperatures, the value of β remains approximately constant as the plasticiser concentration increases, and lies between 0 and 1, which is expected for amorphous systems. As expected, the relaxation times are significantly longer at lower temperature, and in both cases they decrease as the plasticiser concentration increases. The variation is much more pronounced at T = 0.61. This indicates that an increase in plasticiser concentration indeed enhances the local polymer mobility.

For the bulk polymer and bulk polymer–plasticiser systems we do not observe crystal nucleation and growth in either the cooled or isothermal systems. We now proceed to investigate how the model filler surfaces induce crystallisation, and how plasticisers affect the homogeneous nucleation and growth of the polymer crystals.

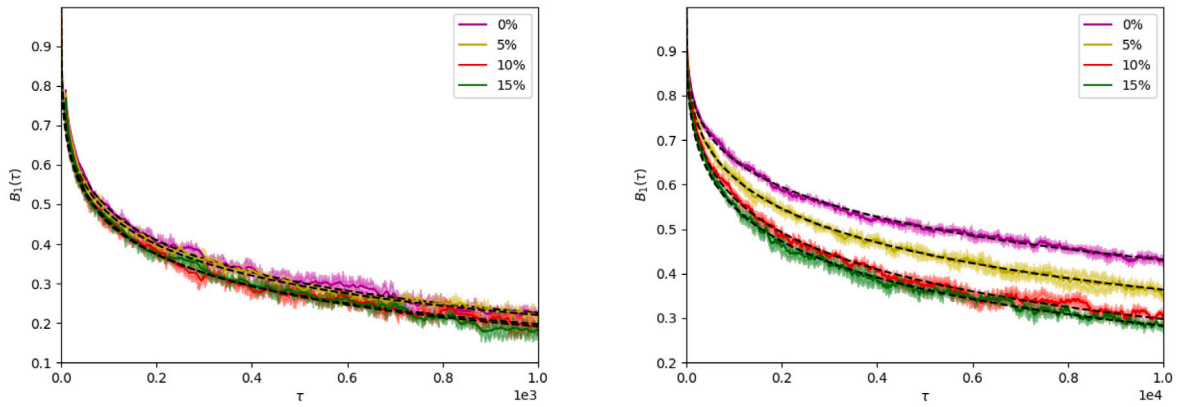

Fig. 2. Dynamical correlation for the central bond in the polymer chains for various plasticiser concentrations in bulk systems at (a) $T = 0.97$ and (b) $T = 0.61$.

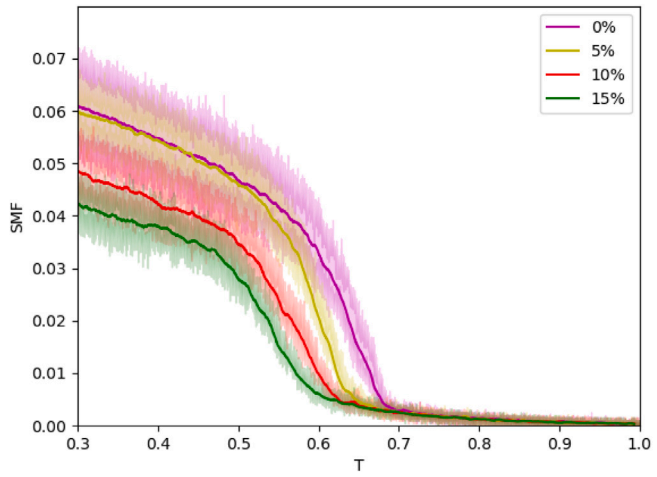

Fig. 3. Stem mass fraction during cooling for plasticiser mass concentration $c_0 = 0\%$, 5%, 10% and 15%. Shaded regions represent the standard error for the respective systems.

Table 1
Fitted KWW parameters for $B_1(\tau)$ data obtained at $T = 0.97$. $\delta\tau_1$ and $\delta\beta$ are the standard errors over the three simulations.

c_0 (%)	τ_1	±	$\delta\tau_1$	β	±	$\delta\beta$
0	286	±	25	0.319	±	0.014
5	263	±	8	0.310	±	0.005
10	210	±	12	0.311	±	0.014
15	212	±	5	0.324	±	0.015

Table 2
Fitted KWW parameters for $B_1(\tau)$ data obtained at $T = 0.61$. $\delta\tau_1$ and $\delta\beta$ are the standard errors over the three simulations.

c_0 (%)	τ_1	±	$\delta\tau_1$	β	±	$\delta\beta$
0	17 200	±	1500	0.300	±	0.012
5	960	±	117	0.310	±	0.006
10	560	±	45	0.330	±	0.011
15	480	±	26	0.320	±	0.006

3.2. Effect of plasticiser concentration on cooling crystallisation at filler surfaces

Polymer–plasticiser systems with model filler surfaces (wall potentials) were studied. These systems were cooled from $T = 1.0$ to $T = 0.3$ at the rate Γ_0 and the variation of stem mass fraction with temperature is shown in Fig. 3. Each cooling curve is an average over 3 independent runs.

In Fig. 3 we can see that the pure polymer system starts to crystallise just below $T = 0.7$, with a rapid increase until just above $T = 0.6$, before giving way to a slower rate of increase until it reaches a stem mass fraction of approximately 0.06 at $T = 0.3$. We note that T_c is slightly higher than that found in our previous work [23], which is due to a different thermal history, as the inclusion of plasticiser required a modification to the equilibration protocol.

As the plasticiser concentration increases, the onset of crystallisation moves to lower temperatures, showing that the degree of undercooling necessary for crystallisation increases with plasticiser concentration, as observed experimentally, for example in PLA plasticised with thermoplastic starch [31] or acetyl triethyl citrate [37], or in PHB plasticised with triacetin or acetyl tributyl citrate [38]. The maximum growth rate, $T_{\max(G)}$, is estimated to occur at temperatures 0.64, 0.60, 0.57, and 0.55 for the $c_0 = 0\%$, 5%, 10% and 15% plasticiser systems, respectively. This is consistent with the previous observations that increasing plasticiser concentration increased local chain mobility of the amorphous polymer, and decreased T_g, which in turn leads to lower T_c and $T_{\max(G)}$. A schematic explanation in terms of free energy is provided in Supporting Information Fig. 1, which will be discussed further below. In future work, it would be interesting to explore the impact of plasticiser–polymer compatibility on the lowering of T_c and $T_{\max(G)}$.

Fig. 3 also shows that higher plasticiser concentrations lead to a decrease in the stem mass fraction at low temperatures. We have seen that, in this work, increasing plasticiser concentration leads to a reduction in both T_g and T_c. The quantity $(T_c - T_g)$ decreases from 0.15 to 0.11 as plasticiser concentration increases, and the polymer dynamics slows down as T_g is approached. In addition, for a constant cooling rate, this reduced temperature range for crystal growth, $(T_c - T_g)$, reduces the time available for the crystals to grow before reaching T_g, resulting in a lower stem mass fraction.

Fig. 4 shows snapshots of the plasticiser systems at $T = 0.3$. We can see that the crystal structure has nucleated only at the bottom wall and grows away from the model filler surface. We also note that the plasticiser is expelled from the crystal into the amorphous region, consistent with experimental observations [33,39]. Since the total number of plasticiser particles within the simulation cell is conserved, the expulsion from crystal regions leads to an increase in the plasticiser concentration within the amorphous region as crystallisation progresses.

3.3. Isothermal crystallisation of plasticiser systems at maximum growth temperatures

To understand further the crystal nucleation and growth process, we now investigate crystallisation using isothermal simulations performed at the respective $T_{\max(G)}$ for each plasticiser concentration. The stem

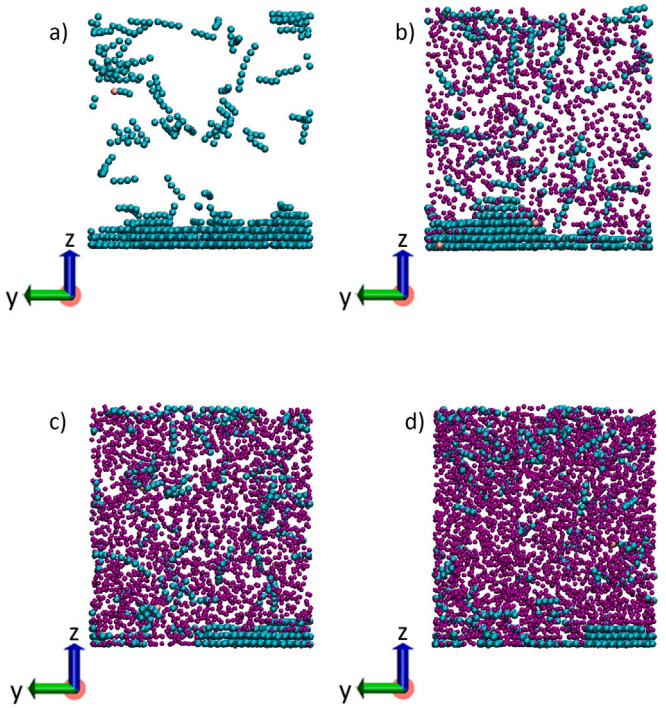

Fig. 4. Simulation snapshots from cooling simulations at $T = 0.3$ show stems (green), chain ends (pink) and plasticiser particles (purple) for (a) pure polymer, (b) $c_0 = 5\%$, (c) $c_0 = 10\%$, and (d) $c_0 = 15\%$.

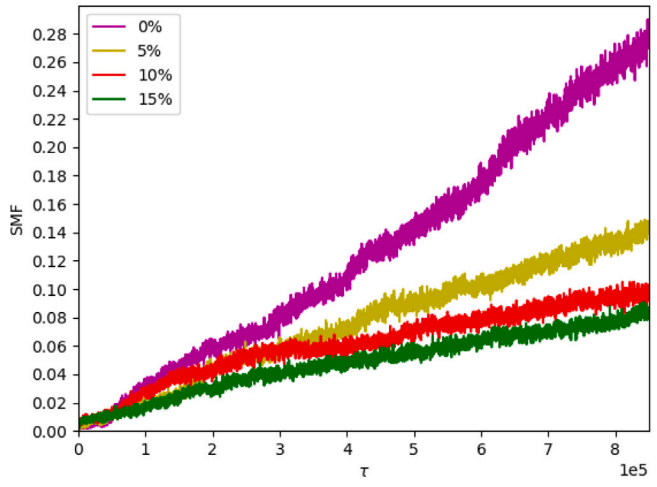

Fig. 5. Stem mass fraction during isothermal NPT simulations for systems with plasticiser mass concentrations $c_0 = 0\%$ at $T = 0.64$, $c_0 = 5\%$ at $T = 0.60$, $c_0 = 10\%$ at $T = 0.57$, and $c_0 = 15\%$ at $T = 0.55$.

mass fraction as a function of time is shown in Fig. 5 for each of the systems, and the final structures are displayed in Fig. 6.

First, we note that the stem mass fraction of the pure polymer system grows approximately linearly with time, except for a few small step increases in growth rate. Visualisation of the simulation shows that two crystal structures nucleated at the bottom wall before $0.5 \times 10^5 \tau$ (data not shown) and by the end of the simulation both structures reached the top surface as shown in Fig. 6(a). For the plasticised systems we can see in Fig. 5 that the growth rate decreases as the plasticiser concentration increases (and corresponding $T_{\max(G)}$ decreases), yielding lower final crystallinity as observed in Fig. 6. For the system with 15% plasticiser two crystal structures also nucleated, the first at $\tau = 0.8 \times 10^5$ and the

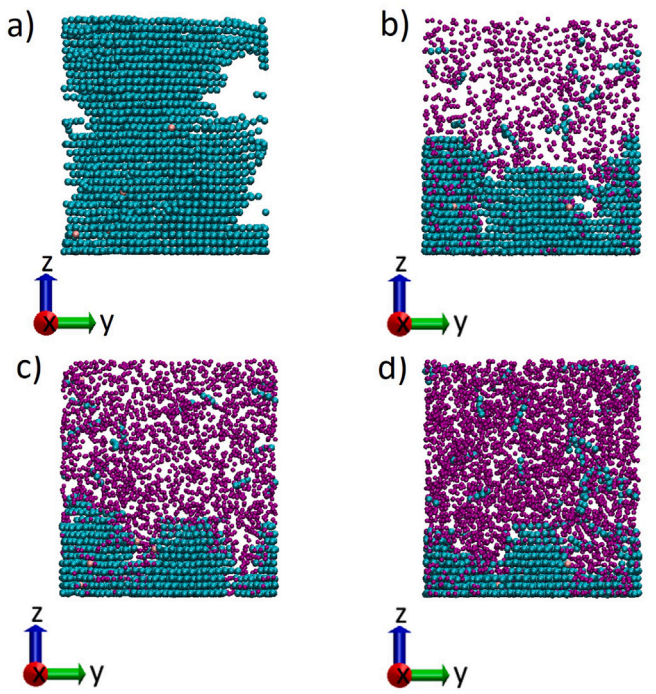

Fig. 6. Snapshots of crystal structures at the end of the isothermal runs at maximum growth temperatures show stems (green), chain ends (pink) and plasticiser beads (purple) with concentration (a) $c_0 = 0\%$ at $T = 0.64$, (b) $c_0 = 5\%$ at $T = 0.60$, (c) $c_0 = 10\%$ at $T = 0.57$, and (d) $c_0 = 15\%$ at $T = 0.55$.

second at $\tau = 1.375 \times 10^5$, however, their growth slows quite early on in the simulation around $\tau = 2 \times 10^5$.

Although it is interesting to study growth at the maximum cooling rate, it is difficult to disentangle the effects of plasticiser concentration and temperature. As the plasticiser concentration increases, T_g and $T_{\max(G)}$ also decrease, with the difference $\Delta T = T_{\max(G)} - T_g$ decreasing from 0.15 for the pure polymer, to 0.11 for the 15% plasticiser system. This means that the isothermal simulations at maximum growth temperature for the latter are closer to the glass transition temperature, and thus we would expect slower chain transport properties and a slower crystal growth rate, from both proximity to T_g and thermal fluctuations.

3.4. Isothermal crystallisation of plasticiser systems at $T = 0.61$

Experimentally, it is common practice to measure isothermal crystal growth at a particular temperature for all systems, and this temperature is typically chosen to be between T_m and T_g. Following this approach, we ran an isothermal simulation at $T = 0.61$ for all plasticiser concentrations. From Fig. 3, it is seen that this temperature is below $T_{\max(G)}$ for the pure polymer and 5% plasticiser systems, but above $T_{\max(G)}$ for the 10% and 15% systems.

The variation with time of the stem mass fraction and the average stem length for the different plasticiser concentrations is shown in Fig. 7. From the stem mass fraction in Fig. 7(a) we observe a significant nucleation induction time for the $c_0 = 15\%$ plasticiser system. At approximately $1.5 \times 10^5 \tau$ the stem mass fraction grows at a fast rate, before slowing slightly from around $4 \times 10^5 \tau$. The $c_0 = 5\%$ and $c_0 = 10\%$ plasticiser systems do not show such a pronounced nucleation induction time, however, they also appear to show a fast growth regime, followed by a slower growth regime. The stem mass fraction for the pure polymer system is lower, making it difficult to determine if it also exhibits faster and slower growth regimes. However, it appears that it also has a measurable nucleation induction time, with a small increase in stem mass fraction at approximately $1.0 \times 10^5 \tau$. The higher crystallinity for

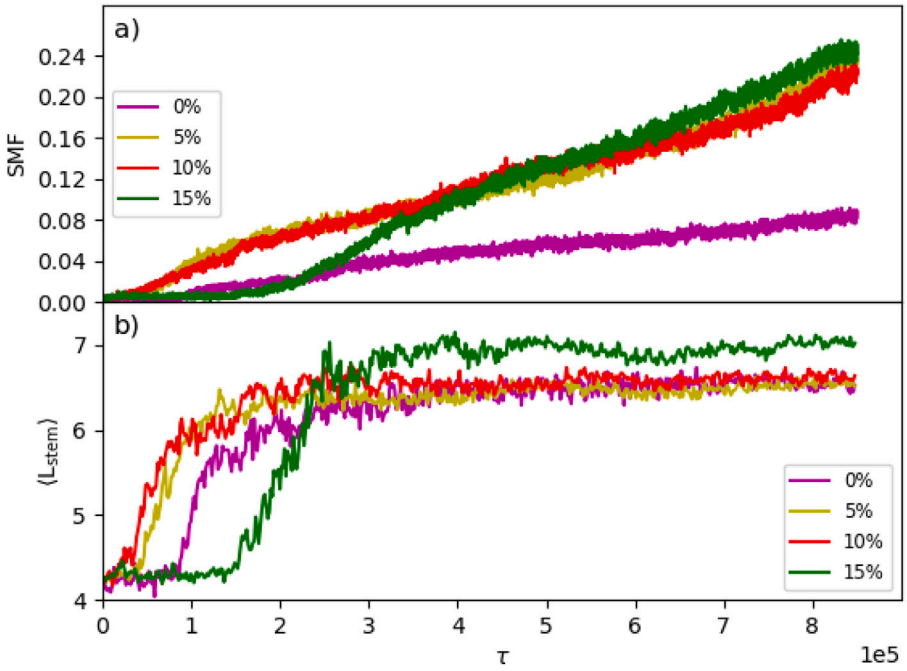

Fig. 7. Isothermal crystallisation for $c_0 = 0\%$, 5%, 10% and 15% at T = 0.61 showing (a) stem mass fraction (SMF), (b) average stem length (in beads).

the plasticised systems compared to the pure polymer has also been observed experimentally [32].

Further insight into the growth regimes is provided by the average stem length variation with time, which is shown in Fig. 7(a). Prior to nucleation, all systems have an average stem length of approximately 4.3, which corresponds to the small number of randomly oriented stems in the amorphous polymer. Furthermore, they all display a rapid increase in average stem length, which appears to be a signature of nucleation. After nucleation begins, we observe that the initial fast growth in stem mass fraction coincides with a significant increase in the average stem length.

After the rapid increase, the average stem length plateaus to an approximately constant average stem length, which is indicative of the crystal thickness. This behaviour of the average stem length during nucleation and growth is similar to observations in a small and wide angle X-ray scattering (SWAXS) study of plasticised PLLA systems [11], and is consistent with the Lauritzen–Hoffman model [40,41]. It is also similar to the rapid growth and plateauing of stem lengths during crystallisation observed in molecular dynamics simulations of polyethylene by Verho et al. [42].

We note that in Fig. 7(a) the steady state value of the average stem length appears larger for the $c_0 = 15\%$ plasticiser system than the others. An increase in lamella thickness with higher plasticiser loading has been observed in the SWAXS study by Diep et al. [11].

In Fig. 8 we show the variation of stem mass fraction, average stem length and crystal height with time for the $c_0 = 15\%$ system, alongside snapshots corresponding to the five times A-E marked on the graphs. For each point there are two snapshots: the x-z plane shows the perpendicular growth of the crystal away from the filler surface, and the x-y plane at $z = 0$ shows the lateral growth across the filler surface.

For clarity, all snapshots display plasticiser beads and stems only. Snapshot A is at $\tau = 0.99 \times 10^5$, when the system is still amorphous before nucleation occurred, and only plasticiser particles and a small number of short randomly orientated stems can be seen. Snapshot B is at $\tau = 1.69 \times 10^5$, and shows an early stage following nucleation. Snapshot C is at $\tau = 2.69 \times 10^5$ which is just after the rapid increase in the average stem length. Here, we see that a single crystal has grown in both the lateral and perpendicular directions. From C to D, we observe only a small change in height, but a large lateral growth of the crystal. From D to E (the end of the simulation) there appears to be a change from lateral growth to perpendicular growth dominating.

Fig. 9 shows the stem mass fraction, average stem length, and height of the crystal for the $c_0 = 5\%$ system. As expected this shows a far shorter nucleation time and different growth rates to the $c_0 = 15\%$ system. In the $c_0 = 5\%$ system, snapshot B shows two crystals nucleating at $0.6 \times 10^5 \tau$, which is just before the rapid increase in average stem length. C is at the end of this rapid growth at $1.28 \times 10^5 \tau$, which corresponds to the lateral extension of the crystals. From C to D, both lateral and perpendicular growth are observed, and after D the crystal growth appears to transition to a perpendicular growth dominated regime, and at the end of the isothermal simulation the crystal has reached a larger height compared to the $c_0 = 15\%$ system.

3.5. Melting of crystal structures

We investigate the melting of the crystal structures grown in the $T = 0.61$ isothermal simulations for $c_0 = 0\%$, 5%, 10% and 15% plasticiser loading. These structures were heated at a rate Γ_0 to T = 0.90, at which point the systems are all in melt states.

Fig. 10(a) shows the variation of stem mass fraction with heating for the different plasticiser systems. For the pure polymer system ($c_0 = 0\%$), the stem mass fraction begins at 0.17 at $T = 0.61$, and fluctuates around a near constant mean value up to $T \approx 0.82$. The average stem length decreases approximately linearly from around 6.3 at $T = 0.61$ to around 5.5 at $T = 0.86$. This slow linear decrease is likely to be due to the mobility of stem chain ends increasing as temperature is increased. The chains are relatively short and a significant proportion of chain ends, which are more mobile, are located at the edge of the crystal, as seen in the snapshots in Fig. 10. The increase in temperature further increases the mobility of the chain ends, which reduces the stem length. However, the stems remain in the crystal phase until T = 0.82, where we see a significant decrease in stem mass fraction. After this point the stem mass fraction drops quickly and reaches zero at $T = 0.86$, when the average stem length also drops sharply to the melt value, indicating melting of the crystal.

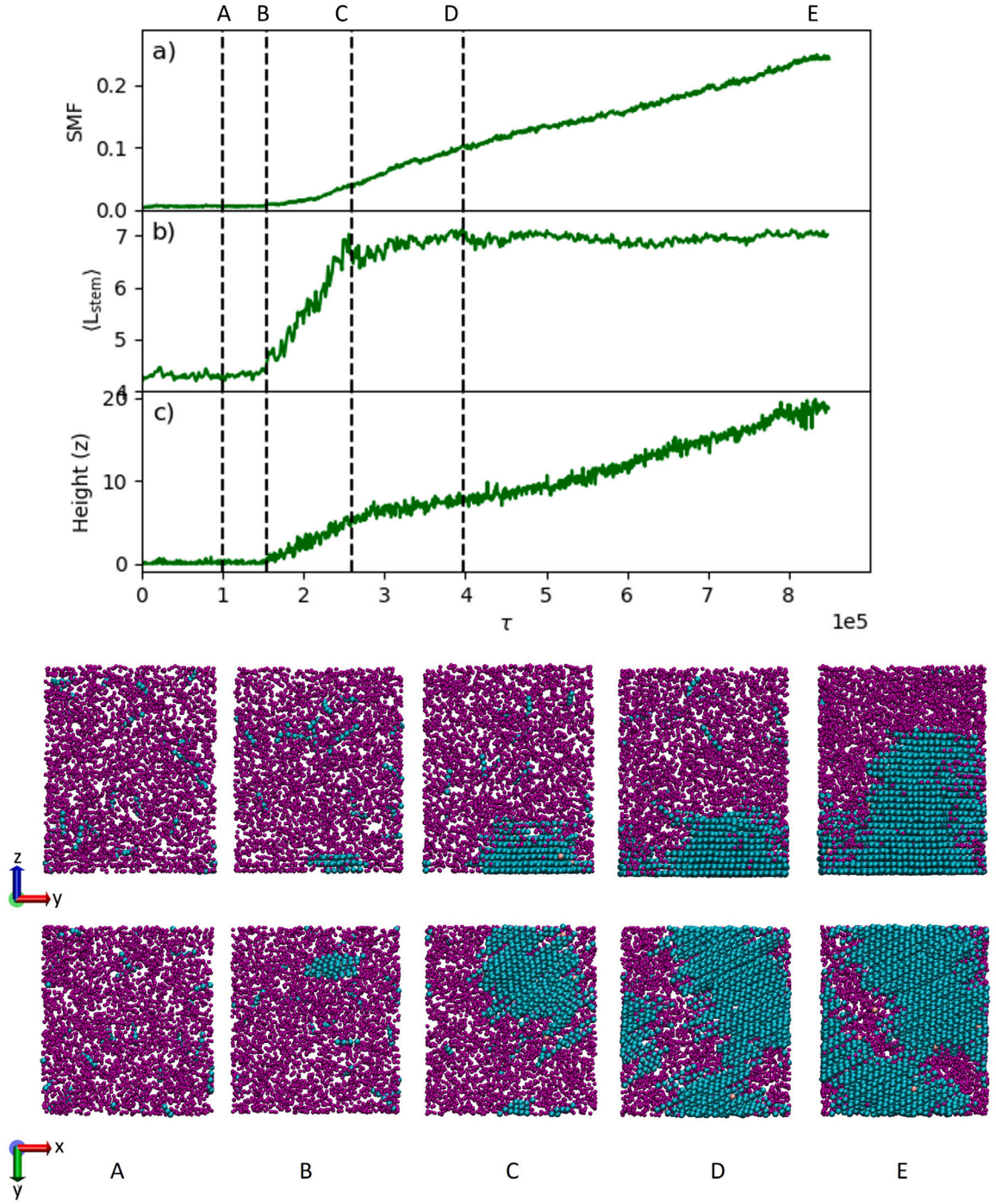

Fig. 8. Variation of (a) stem mass fraction, (b) average stem length, and (c) crystal height with time during an isothermal simulation for $c_0 = 15\%$. The snapshots show stems and plasticisers for cross sections in the x-z plane (top row) and the x-y plane at $z = 0$ (bottom row) for the points on the graph labelled A to E.

For the $c_0 = 5\%$, 10% and 15% systems, we also see that the average stem length decreases slowly and linearly before exhibiting rapid drops when the systems completely melt. The temperature at which complete melting occurs, T_{m0}, is seen to decrease as c_0 increases, as observed in experiments [10–12,43].

We also note that the shape of the stem mass fraction curve during heating for the plasticiser systems is different to that of the pure system. For the pure polymer, the stem mass fraction fluctuates around a near constant mean before decreasing rapidly to zero at around T_{m0}, which would be expected for a first order phase transition. However, in the plasticiser systems, it can be seen that the stem mass fraction slowly decreases to zero, with an apparent broadening of the melting regime. Melting point widening has been observed in DSC curves for addition of plasticising PLA monomers into PLA [13] (see Fig. 1) and for addition of acetyl tributyl citrate plasticiser in PHB [10].

In Fig. 10 we have included simulation snapshots for the $c_0 = 15\%$ plasticiser system at temperatures 0.61, 0.65, 0.69, 0.72, and 0.78. Between the temperatures 0.61 to 0.69 the crystal height does not change significantly, however, above $T = 0.69$ the height of the crystal starts decreasing visibly, correspond to a more rapid drop in the stem mass fraction. Visualisation of the simulation shows that as the temperature increases, the stems start to peel off the crystal in

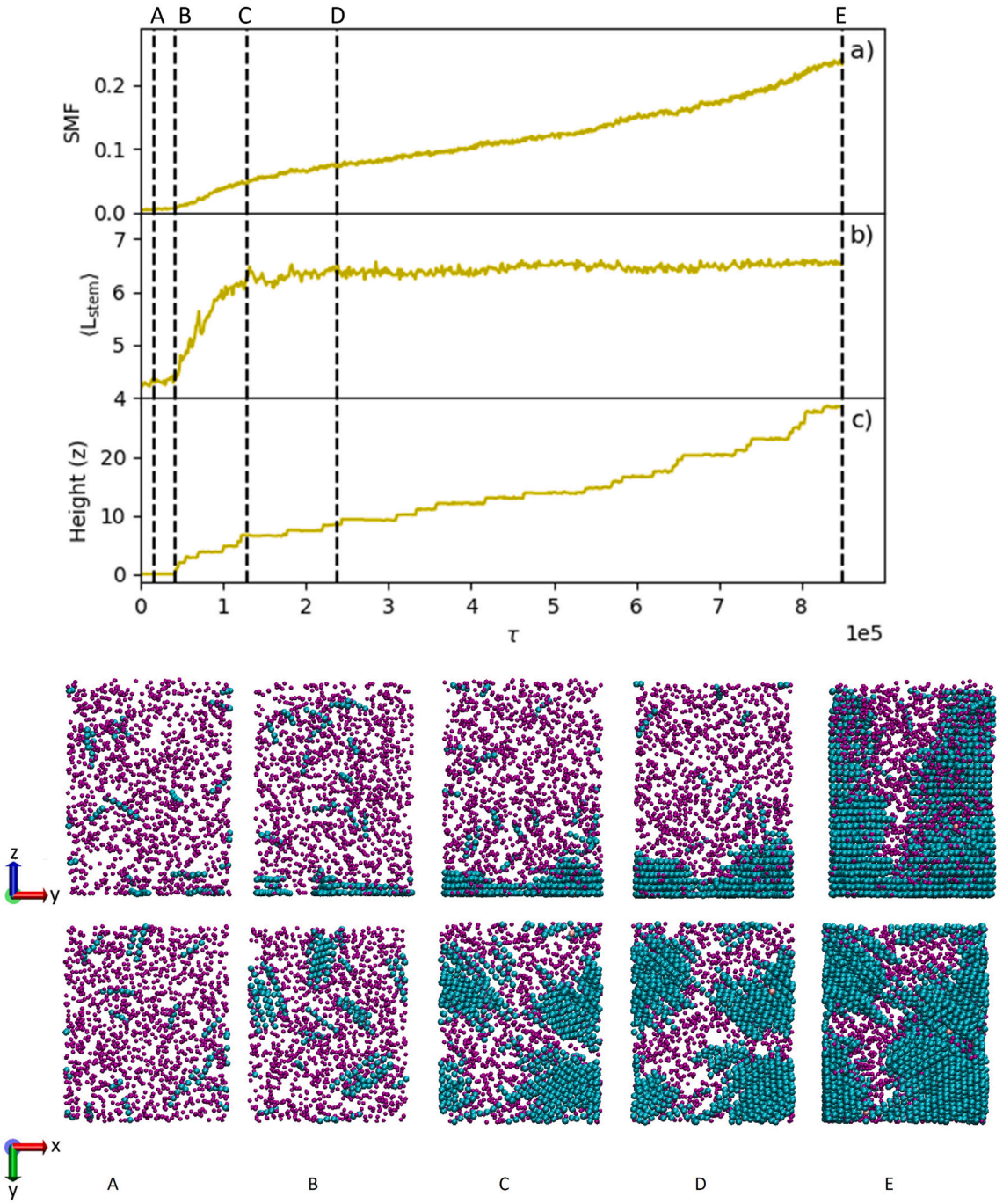

Fig. 9. The graph shows (a) stem mass fraction, (b) average stem length and (c) crystal height in the z-direction during an isothermal NPT simulation for $c_0 = 5\%$. The snapshots show stems (green), chain ends (pink) and plasticiser beads (purple) for cross sections in the x-z plane (top row) and the x-y plane at $z = 0$ (bottom row) for the points on the graph labelled A to E.

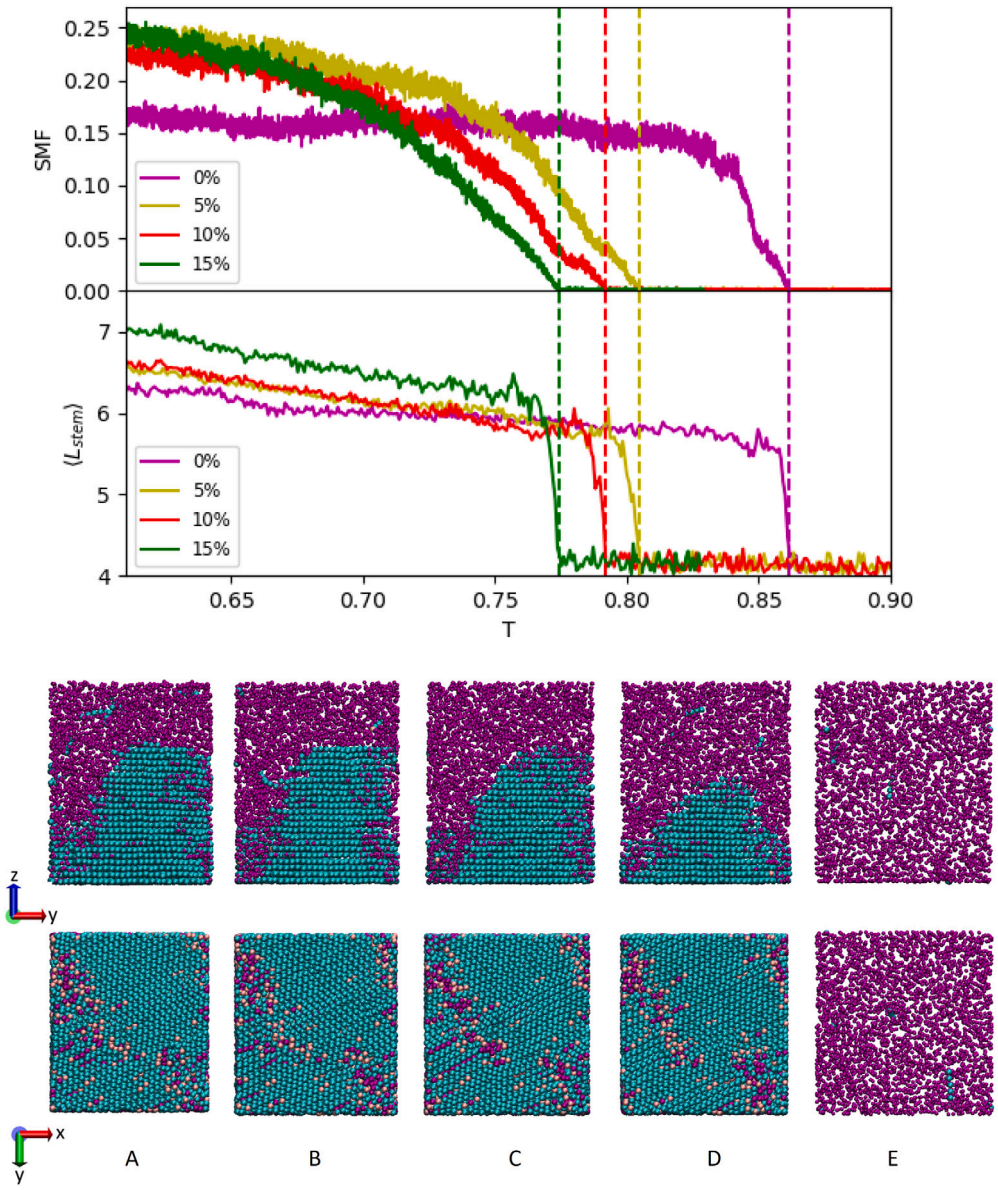

Fig. 10. The graph shows (a) stem mass fraction, and (b) average stem length during heating from $T = 0.61$ at a heating rate of Γ_0 for $c_0 = 0\%$, 5%, 10% and 15%. The dashed lines indicate the melting temperatures in each system. The snapshots A-E show stems (green), chain ends (pink), and plasticiser beads (purple) for the $c_0 = 15\%$ system for cross sections in the x-z plane (top row) and the x-y plane at z = 0 (bottom row) at temperatures of 0.61, 0.65, 0.69, 0.72, and 0.78, respectively.

a layer-by-layer fashion, thus decreasing the stem mass fraction. This apparent melting of stem layers occurs at the top of the crystal structure furthest away from the filler surface. Between T = 0.72 and T = 0.78 the crystal has completely melted, and the stem mass fraction goes to zero at around $T_{m0} = 0.77$.

We can explain this broadening of the melting regime by the changing equilibrium conditions as the crystal melts, which results in a changing plasticiser concentration in the amorphous regime. As a stem layer peels off, the crystal structure that is left behind is in (or is close to) equilibrium with the amorphous phase for that particular temperature and plasticiser concentration. Recall that no plasticiser resides in the crystal phase, so that as the crystal melts, the plasticiser concentration in the amorphous phase decreases with a concommitant increase in the Gibbs free energy of that phase. The remaining smaller crystalline structure persists until the temperature has increased sufficiently so that it is no longer the stable structure, whence another layer peels away leading to a further decrease in plasticiser concentration. This process is repeated until the final structure melts at the filler surface resulting in the abrupt reduction in the average stem length.

Following this argument, we can equate the amorphous and crystal free energies for a fixed overall diluent concentration, to relate the variation of crystal fraction to temperature. This gives the following expression for the dependence of the fractional crystallinity $X(T)$ on temperature T for plasticiser systems (see Supporting Information for details):

$$X(T) = \frac{\delta T}{c_0/A + \delta T}, \quad \delta T > 0 \tag{8}$$

Here $\delta T = T_{m0} - T$, where T_{m0} is the temperature at which the crystal completely melts; $\delta T \ll T_{m0}$. A and T_{m0} depend on the plasticiser concentration in the melt state c_0, as well as on thermodynamic parameters such as specific heats and chemical potential at T_{m0}.

In Fig. 11 the stem mass fraction vs temperature data is plotted against X from Eq. 8, treating A and T_{m0} as fitting parameters. The values of these parameters are reported in Table 3.

The fits are satisfactory in the regime where the layer-by-layer stem melting is observed in Fig. 10. The value of T_{m0} decreases with increasing concentration, and as expected are higher than the temperatures at

Table 3
Fitting parameters A and T_{m0} obtained from fitting to heating data for plasticiser concentrations 5%, 10% and 15%.

c_0 (%)	T_m	A	A/c_0
5	0.804	0.277	5.54
10	0.792	0.342	3.42
15	0.775	0.341	2.27

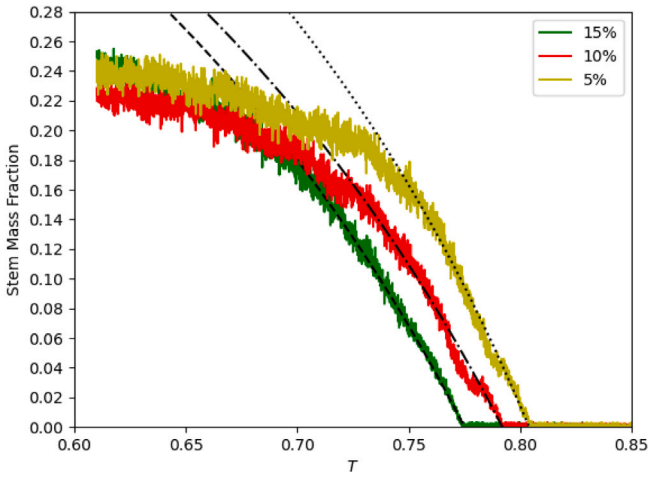

Fig. 11. Variation of stem mass fraction with temperature, and fits to Eq. (8).

which crystallisation occurs upon cooling in Fig. 3, due to the excess free energy of critical nuclei [23]. The parameter A increases from 5% to 10% but does not change when the concentration is increased to 15%. However the ratio A/c_0 decreases with increasing plasticiser concentration, where the ratio A/c_0 controls the crystal fraction on melting for small dT. The thermodynamic coefficient A is the ratio of the difference in heat capacities between the amorphous and crystalline phase to the chemical potential of the amorphous phase.

4. Summary and conclusions

In this work we have studied the effects of plasticiser on a linear polymer using molecular dynamics simulations of a modified KG model. The results of the study resonate with reported experimental results for a range of polymers.

Firstly, for bulk systems we found that the plasticiser lowered the glass transition temperature Tg, with the size of the temperature depression increasing with plasticiser concentration. This behaviour was correlated with the increased polymer mobility in the plasticised systems.

Secondly, simulating the polymer in contact with a model filler surface, which acts as a nucleant, we found that the plasticiser lowers the crystallisation temperature of the polymer. In cooling simulations, the temperature at which crystallisation occurred lowered with increasing plasticiser concentration, as did the temperature at which the maximum crystallisation growth rate occurred. In isothermal simulations, we observed that crystal nucleation can be delayed by the plasticiser, but regardless the crystal growth followed a specific pattern: firstly nucleation precedes a phase of lateral growth at the surface, thereafter the crystal grows normal to the surface. The stages of growth have been characterised by the average stem length within the crystal, which clearly demonstrates that the crystals evolve to a preferred constant thickness, in accordance with the prevailing Lauritzen–Hoffman model.

Thirdly, we studied crystal melting in the plasticised systems. The most striking feature is that, because the plasticiser remains in the amorphous phase, the effective plasticiser concentration in this phase varies with the degree of crystallinity in the system. In particular, the melting curve for a plasticised system is no longer characterised by a sharp first order phase transition, but instead is broadened across a wide range of temperature. This is due to the impact the plasticiser concentration has on the free energy density of the amorphous phase, which increases as the crystal melts. Consequently, the crystals melt in a layer-by-layer fashion at the uppermost interface with the amorphous phase, away from the filler surface.

Experimentally, plasticiser content has been shown to decrease T_c to lower temperatures and to have an effect on the number density of spherulites, for example as seen in PHB films [6] as well as changing the spherulite growth rate. In this work, we developed a model that captures essential properties such as a depression in T_c as well as changes in crystal growth kinetics seen in isothermal simulations. This highlights the importance of developing a model that is able to capture the essential physics involved in plasticiser addition and its effect on crystallisation.

The significance of these results is two-fold. Firstly, it provides a coherent explanation for experimental results for a range of linear polymers, where fillers and plasticisers are used to improve processability and properties such as mechanical strength and barriers to gas diffusion. Secondly, the model provides a framework to help design the properties of new plastics based on renewable polymers. It is well-recognised that the renewables will have to at least match the performance of traditional oil-based plastics, where process routes and properties have been optimised at scale over decades. This presents a significant challenge, one that it is hoped can be met through a concerted effort to understand and control crystallinity and its development during manufacturing processes. Although this work used a generic polymer model, it is possible to map it to specific linear polymers through the chain stiffness e.g. by matching the Kuhn length [44] meaning that the findings are transferable to a wide range of polymeric systems, including PLA and PHB. In future work we believe that the developed model can be used to guide filler and plasticiser selection for the optimisation and control of crystal properties of renewable polymers.

CRediT authorship contribution statement

Dominic Wadkin-Snaith: Writing – original draft, Visualization, Methodology, Investigation, Formal analysis. **Paul A. Mulheran:** Writing – review & editing, Supervision, Resources, Funding acquisition, Conceptualization. **Karen Johnston:** Writing – review & editing, Writing – original draft, Supervision, Resources, Project administration, Funding acquisition, Data curation, Conceptualization.

Declaration of competing interest

The authors declare that they have no known competing financial interests or personal relationships that could have appeared to influence the work reported in this paper.

Data availability

LAMMPS input files underpinning this work are openly available from the University of Strathclyde KnowledgeBase at https://doi.org/10.15129/3d50ebe5-fc32-4c6a-ade0-b2fbbe054b51. Supplementary information supporting this work is also available.

Acknowledgements

The authors would like to thank Katarzyna Majerczak, Vitor Mague ijo and John Liggat for valuable discussions. The authors gratefully acknowledge funding from a UKRI Smart Sustainable Plastic Packaging grant (NE/V010603/1). Results were obtained using the ARCHIE-WeSt High Performance Computer (www.archie-west.ac.uk) based at the University of Strathclyde.

Appendix A. Supplementary information

Supplementary information presenting the thermodynamic argument for melting point broadening by plasticisers can be found online at https://doi.org/10.1016/j.polymer.2024.127095.

References

[1] Guili Zhao, Xiaomei Lyu, Jaslyn Lee, Xi Cui, Wei-Ning Chen, Biodegradable and transparent cellulose film prepared eco-friendly from durian rind for packaging application, Food Packag. Shelf Life 21 (2019) 100345.

[2] R.A. Ilyas, S.M. Sapuan, Abudukeremu Kadier, Mohd Sahaid Kalil, Rushdan Ibrahim, M.S.N. Atikah, N. Mohd Nurazzi, A. Nazrin, C.H. Lee, Mohd Nor Faiz Norrrahim, Nasmi Herlina Sari, Edi Syafri, Hairul Abral, Latifah Jasmani, M.I.J. Ibrahim, Chapter 8 properties and characterization of PLA, PHA, and other types of biopolymer composites, in: Faris M. Al-Oqla, S.M. Sapuan (Eds.), Advanced Processing, Properties, and Applications of Starch and Other Bio-Based Polymers, Elsevier, 2020, pp. 111–138.

[3] A.O. Pérez-Arauz, A.E. Aguilar-Rabiela, A. Vargas-Torres, A.-I. Rodríguez-Hernández, N. Chavarría-Hernández, B. Vergara-Porras, M.R. López-Cuellar, Production and characterization of biodegradable films of a novel polyhydroxyalkanoate (PHA) synthesized from peanut oil, Food Packag. Shelf Life 20 (2019) 100297.

[4] Feng Wu, Manjusri Misra, Amar K. Mohanty, Challenges and new opportunities on barrier performance of biodegradable polymers for sustainable packaging, Prog. Polym. Sci. 117 (2021) 101395.

[5] Katarzyna Majerczak, Dominic Wadkin-Snaith, Vitor Magueijo, Paul Mulheran, John Liggat, Karen Johnston, Polyhydroxybutyrate: a review of experimental and simulation studies of the effect of fillers on crystallinity and mechanical properties, Polym. Int. 71 (2022) 1398–1408.

[6] Katarzyna Majerczak, John Liggat, Evaluation of spherulite growth in PHB-based systems – A DoE approach, J. Appl. Polym. Sci. 140 (40) (2023) e54469.

[7] Irene Teresita Seoane, Liliana Beatriz Manfredi, Viviana Paola Cyras, Effect of two different plasticizers on the properties of poly(3-hydroxybutyrate) binary and ternary blends, J. Appl. Polym. Sci. 135 (12) (2018) 46016.

[8] Melissa Gurgel Adeodato Vieira, Mariana Altenhofen da Silva, Lucielen Oliveira dos Santos, Marisa Masumi Beppu, Natural-based plasticizers and biopolymer films: A review, Eur. Polym. J. 47 (3) (2011) 254–263.

[9] Muhammed L. Sanyang, Salit M. Sapuan, Mohammad Jawaid, Mohamad R. Ishak, Japar Sahari, Effect of plasticizer type and concentration on tensile, thermal and barrier properties of biodegradable films based on sugar palm (Arenga pinnata) starch, Polymers 7 (6) (2015) 1106–1124.

[10] Denis Mihaela Panaitescu, Cristian Andi Nicolae, Adriana Nicoleta Frone, Ioana Chiulan, Paul Octavian Stanescu, Constantin Draghici, Michaela Iorga, Mona Mihailescu, Plasticized poly(3-hydroxybutyrate) with improved melt processing and balanced properties, J. Appl. Polym. Sci. 134 (19) (2017).

[11] Pham Thi Ngoc Diep, Hideaki Takagi, Nobutaka Shimizu, Noriyuki Igarashi, Sono Sasaki, Shinichi Sakurai, Effects of loading amount of plasticizers on improved crystallization of poly (L-lactic acid), J. Fiber Sci. Technol. 75 (8) (2019) 99–111.

[12] Jyongsik Jang, Dong Kweon Lee, Plasticizer effect on the melting and crystallization behavior of polyvinyl alcohol, Polymer 44 (26) (2003) 8139–8146.

[13] N. López-Rodríguez, J.R. Sarasua, Plasticization of poly-L-lactide with L-lactide, D-lactide, and D,L-lactide monomers, Polym. Eng. Sci. 53 (10) (2013) 2073–2080.

[14] Xia Gao, Shunxin Qi, Bo Yang, Yunlan Su, Jing Li, Dujin Wang, Synergistic effect of plasticizer and nucleating agent on crystallization behavior of polylactide during fused filament fabrication, Polymer 215 (2021) 123426.

[15] Hanwen Xiao, Li Yang, Xiaomin Ren, Tao Jiang, Jen-Taut Yeh, Kinetics and crystal structure of poly(lactic acid) crystallized nonisothermally: Effect of plasticizer and nucleating agent, Polym. Compos. 31 (12) (2010) 2057–2068.

[16] N. Waheed, M.S. Lavine, G.C. Rutledge, Molecular simulation of crystal growth in n-eicosane, J. Chem. Phys. 116 (2002) 2301–2309.

[17] N. Waheed, M.J. Ko, G.C. Rutledge, Molecular simulation of crystal growth in long alkanes, Polymer 46 (20) (2005) 8689–8702.

[18] Takashi Yamamoto, Molecular dynamics modeling of polymer crystallization from the melt, Polymer 45 (4) (2004) 1357–1364.

[19] F. Varnik, J. Baschnagel, K. Binder, Reduction of the glass transition temperature in polymer films: A molecular-dynamics study, Phys. Rev. E (2002).

[20] Paul Z. Hanakata, Jack F. Douglas, Francis W. Starr, Local variation of fragility and glass transition temperature of ultra-thin supported polymer films, J. Chem. Phys. 137 (2012) 244901.

[21] Mark E. Mackura, David S. Simmons, Enhancing heterogenous crystallization resistance in a bead-spring polymer model by modifying bond length, J. Polym. Sci. B 52 (2) (2014) 134–140.

[22] Chuanfu Luo, Martin Kröger, Jens-Uwe Sommer, Molecular dynamics simulations of polymer crystallization under confinement: Entanglement effect, Polymer 109 (2017) 71–84.

[23] Dominic Wadkin-Snaith, Paul Mulheran, Karen Johnston, Filler-induced heterogeneous nucleation of polymer crystals investigated by molecular dynamics simulations, Polymer 281 (2023) 126113.

[24] Giuliana Giunta, Lois Smith, Kristof Bartha, H. Ali Karimi-Varzaneh, Paola Carbone, Understanding the balance between additives' miscibility and plasticisation effect in polymer composites: a computational study, Soft Matter 19 (2023) 2377–2384.

[25] Jayachandra Hari Mangalara, David S. Simmons, Tuning polymer glass formation behavior and mechanical properties with oligomeric diluents of varying stiffness, ACS Macro Lett. 4 (10) (2015) 1134–1138.

[26] David S. Simmons, Jack F. Douglas, Nature and interrelations of fast dynamic properties in a coarse-grained glass-forming polymer melt, Soft Matter (2011) 11010–11020.

[27] Evgeny B. Stukalin, Jack F. Douglas, Karl F. Freed, Plasticization and antiplasticization of polymer melts diluted by low molar mass species, J. Chem. Phys. 132 (8) (2010).

[28] Aidan P. Thompson, H. Metin Aktulga, Richard Berger, Dan S. Bolintineanu, W. Michael Brown, Paul S. Crozier, Pieter J. in 't Veld, Axel Kohlmeyer, Stan G. Moore, Trung Dac Nguyen, Ray Shan, Mark J. Stevens, Julien Tranchida, Christian Trott, Steven J. Plimpton, LAMMPS - a flexible simulation tool for particle-based materials modeling at the atomic, meso, and continuum scales, Comput. Phys. Comm. 271 (2022) 108171.

[29] William Humphrey, Andrew Dalke, Klaus Schulten, VMD – Visual Molecular Dynamics, J. Mol. Graph. 14 (1996) 33–38.

[30] Christoph Bennemann, Wolfgang Paul, Jörg Baschnagel, Kurt Binder, Investigating the influence of different thermodynamic paths on the structural relaxation in a glass-forming polymer melt, J. Phys.: Condens. Matter 11 (10) (1999) 2179.

[31] O. Martin, L. Avérous, Poly(lactic acid): plasticization and properties of biodegradable multiphase systems, Polymer 42 (14) (2001) 6209–6219.

[32] Nadia Ljungberg, Bengt Wesslén, The effects of plasticizers on the dynamic mechanical and thermal properties of poly(lactic acid), J. Appl. Polym. Sci. 86 (5) (2002) 1227–1234.

[33] E. Piorkowska, Z. Kulinski, A. Galeski, R. Masirek, Plasticization of semicrystalline poly(l-lactide) with poly(propylene glycol), Polymer 47 (20) (2006) 7178–7188, Containing: Structure and Dynamics of Complex Polymeric Materials. Commemorating Tadeusz Pakula.

[34] Cecile Courgneau, Sandra Domenek, Regis Lebosse, Alain Guinault, Luc Avelino Cormarous, Violette Ducruet, Effect of crystallization on barrier properties of formulated polylactide, Polym. Int. 61 (2) (2012) 180–189.

[35] Ana Chaos, Ainara Sangroniz, Jorge Fernandez, Javier del Rio, Marian Iriarte, Jose Ramon Sarasua, Agustin Etxeberria, Plasticization of poly(lactide) with poly(ethylene glycol): Low weight plasticizer vs triblock copolymers. Effect on free volume and barrier properties, J. Appl. Polym. Sci. 137 (28) (2020) 48868.

[36] David McKechnie, Jordan Cree, Dominic Wadkin-Snaith, Karen Johnston, Glass transition temperature of a polymer thin film: Statistical and fitting uncertainties, Polymer 195 (2020) 122433.

[37] Hongbo Li, Michel A. Huneault, Effect of nucleation and plasticization on the crystallization of poly(lactic acid), Polymer 48 (23) (2007) 6855–6866.

[38] Katarzyna Majerczak, John J. Liggat, Submission to journal of polymers and the environment evaluation of thermal properties and crystallinity in PHB-based systems –A DoE approach, J. Polym. Environ. (2024/04/14).

[39] N. Varol, N. Delpouve, S. Araujo, S. Domenek, A. Guinault, R. Golovchak, A. Ingram, L. Delbreilh, E. Dargent, Amorphous rigidification and cooperativity drop in semi-crystalline plasticized polylactide, Polymer 194 (2020) 122373.

[40] J.I. Lauritizen Jr., J.D. Hoffman, Theory of formation of polymer crystals with folded chains in dilute solution, J. Res. Natl. Bur. Stand. 64A(1) (73–102) (1960).

[41] Buckley Crist, Jerold M. Schultz, Polymer spherulites: A critical review, Prog. Polym. Sci. 56 (2016) 1–63.

[42] Tuukka Verho, Antti Paajanen, Jukka Vaari, Anssi Laukkanen, Crystal growth in polyethylene by molecular dynamics: The crystal edge and lamellar thickness, Macromolecules 51 (13) (2018) 4865–4873, 30258252.

[43] Rogerio Ramos de Sousa Junior, Carlos Alberto Soares dos Santos, Nathalie Minako Ito, Airton Nizetti Suqueira, Maximilian Lackner, Demetrio Jackson dos Santos, PHB processability and property improvement with linear-chain polyester oligomers used as plasticizers, Polymers 14 (19) (2022).

[44] Ralf Everaers, Sathish K. Sukumaran, Gary S. Grest, Carsten Svaneborg, Arvind Sivasubramanian, Kurt Kremer, Rheology and microscopic topology of entangled polymeric liquids, Science 303 (2004) 823.